Assessment of basin-wise future agricultural drought status across India under changing climate

Mayank Suman and Rajib Maity

ABSTRACT

Most of the existing studies on meteorological drought suggest more intense and frequent drought events due to changing climate. However, basin-scale assessment of future agricultural drought is lacking due to many reasons. In this study, the intensity and frequency of future agricultural drought (characterized by the Standardized Soil Moisture Index, SSMI) for 226 sub-basins across India are analyzed, and vulnerable basins are identified. The prediction of the future agricultural drought status is achieved using the wavelet-based drought temporal consequence modeling of meteorological drought with the best performing bias-corrected Coordinated Regional Downscaling Experiment (CORDEX) simulations, selected by Multi-Criteria Decision-Making frameworks. This study reveals a geographically contrasting change in future agricultural drought that indicates more intense agricultural drought in north, north-east, and central India as compared with south India. The area under drought is also expected to increase, and about 20 and 50% of the Indian mainland is expected to suffer from extreme (SSMI ≤ -2) and moderate (SSMI ≤ -1) agricultural drought conditions by the end of this century. Sub-basins lying in north and central India are expected to have a longer time under drought conditions. Thus, the findings of this study will be useful for future planning and preparedness against agricultural productivity.

Key words | agricultural drought, climate change, Coordinated Regional Downscaling Experiment (CORDEX), future assessment, Standardized Soil Moisture Index (SSMI)

Mayank Suman
School of Water Resources,
Indian Institute of Technology,
Kharagpur,
India

Rajib Maity (corresponding author)
Department of Civil Engineering,
Indian Institute of Technology,
Kharagpur,
India
E-mail: *rajib@civil.iitkgp.ernet.in*;
rajib@civil.iitkgp.ac.in

HIGHLIGHTS

- Future agricultural drought status reveals new insights into its spatial variation.
- The concept of drought translation is a useful one for making use of the best potential of climate model simulations.
- More intense droughts in north, north-east and central India are expected as compared with south India.
- In future, about 20 and 50% of the area in India is expected to face extreme and moderate agricultural droughts, respectively.

doi: 10.2166/wcc.2021.369

GRAPHICAL ABSTRACT

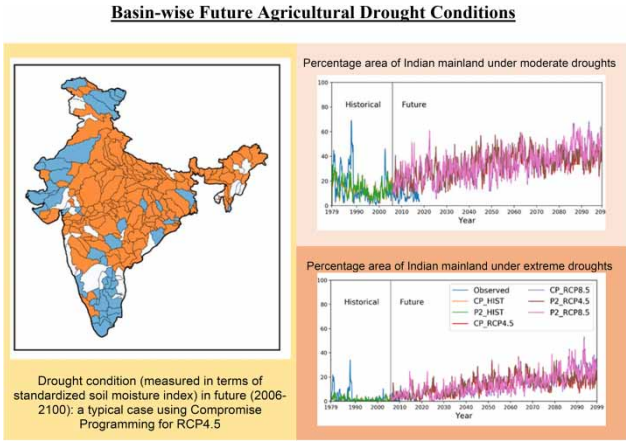

INTRODUCTION

Agricultural drought is defined as a prolonged period of soil moisture deficit, which affects agricultural production. For a country like India, which is heavily dependent on agricultural economy (constituting 16% of the gross domestic product according to the Ministry of Finance, India (2018)), agricultural droughts have a significant impact on its socio-economic well-being. Hence, monitoring, assessment, and prediction of agricultural drought are of immense importance. With prior knowledge of vulnerable regions in terms of drought propensity, policies/plans can be developed to mitigate the adverse effects of agricultural drought.

Previous studies suggest that, in general, drought risk has increased globally (Dai *et al.* 2004; Dai 2011; Vicente-Serrano *et al.* 2014; Wang *et al.* 2015; Xu *et al.* 2015; Zhao *et al.* 2018). However, some studies suggest no significant or little change in observed drought series (Seneviratne *et al.* 2012; Sheffield *et al.* 2012; Greve *et al.* 2014). While there might not be a consensus for the past, the research community largely agrees with the expected future changes in drought conditions globally. With the changing climate, air temperature is expected to increase, resulting in a drying tendency in soil moisture and stream flow (Trenberth *et al.* 2003; Trenberth 2011; Annamalai *et al.* 2013) along with higher and intense precipitation (Maity *et al.* 2016a). Due to these future changes, more intense and frequent droughts along with an increase in the area under drought are predicted (Sheffield & Wood 2008; Dai 2011, 2013; Field *et al.* 2012; Stocker *et al.* 2013). Additionally, flash droughts (drought events with rapid onset primarily due to intense heat waves) are expected to become more common in the future (Gerken *et al.* 2018; Yuan *et al.* 2019). Many regional studies suggest that drought is expected to become more severe and frequent, and areas under drought are expected to increase with local variation in the future (Burke & Brown 2010; Chen & Sun 2017; Kang & Sridhar 2017; Spinoni *et al.* 2018). For instance, according to Burke & Brown (2010), the intensity and frequency of droughts may increase over the entire UK with regional variation, but it is difficult to ascertain whether these changes will result from natural variability or from the effect of the changing climate. According to Chen & Sun (2017), the drought severity, frequency, and duration are expected to increase in the future in eastern China. Similarly, the severity and frequency of droughts in Europe are expected to increase with spatio-temporal variations due to the changing climate (Spinoni *et al.* 2018). Hence, the spatio-temporal distribution of drought and risk, thereof, are nonuniform with local variations under changing climate, which, if understood well, can help in managing/mitigating the future droughts (Thomas *et al.* 2015; Xu *et al.* 2015).

In the Indian context, the characterization of drought has been attempted in multiple studies (Mishra & Singh 2009; Pai *et al.* 2011; Naresh *et al.* 2012; Ojha *et al.* 2013;

Mishra *et al.* 2014; Thomas *et al.* 2015; Mallya *et al.* 2016; Sharma & Mujumdar 2017; Zhang *et al.* 2017; Bisht *et al.* 2019). According to Mishra & Singh (2009), meteorological drought in the Kansawati basin is expected to become more severe and frequent. Pai *et al.* (2011), in their district-wise analysis of drought conditions using the seasonal Standardized Precipitation Index (SPI), found that there is spatial variation in drought characteristics throughout India. For instance, most districts in north and central India show an aggravating meteorological drought condition; however, most districts in south and west India show a decreasing risk of meteorological drought. Naresh *et al.* (2012) reported an increase in drought severity across India using the SPI as a meteorological drought index. An analysis of multiple meteorological drought indices by Mallya *et al.* (2016) and an analysis of the spatial extent of concurrent meteorological droughts and heatwaves by Sharma & Mujumdar (2017) using observed data suggested that, along with an increase in drought severity and frequency across India in the past, droughts are also becoming more regional in nature. According to them, the most affected regions are coastal south India, central Maharashtra, and the Indo-Gangetic plain, all being major agricultural areas. Zhang *et al.* (2017) suggested an increase in drought severity over the wheat-growing areas of India and estimated its impact on wheat production. Bisht *et al.* (2019) analyzed future meteorological drought and reported that despite a long-term increase in drought severity and intensity across the Indian mainland, regional variations in these drought characteristics are expected.

Most of the above-mentioned studies analyzed meteorological drought using indices, such as the SPI, the Standardized Precipitation Evapotranspiration Index (SPEI), and the Palmer Drought Severity Index (PDSI), using coarse resolution data (usually from General Circulation Models (GCMs)) in the future. A pan-India, basin-wise assessment of future agricultural drought across all basins is lacking. To address this issue, the use of finer resolution is necessary to reveal a local variation in drought condition(s) in a better way from many perspectives. Additionally, the fine-resolution analysis of soil moisture deficit may help in assessing other climatic variables, as the soil moisture is expected to have a feedback to many climatic variables/phenomena, such as heatwave (Hirabayashi *et al.* 2013; D'Andrea *et al.* 2016), monsoon in Asia and Africa (Douville 2002), summer air temperature (Douville *et al.* 2016), and others. A large-scale assessment of agricultural drought is also important from the food security point of view. Thus, the objectives of this study are to analyze the change in the intensity and frequency of future agricultural drought across India, divided into 226 sub-basins, and to identify the vulnerable basins/regions. The Standardized Soil Moisture Index (SSMI) is used as the drought characterizing index.

The rest of the article is organized as follows. In the next section, details of the study area, showing the river basins and sub-basins across India, and data used are presented. In the section 'Methodology', details of the methodological approach are outlined. In the subsequent 'Results and discussion' section, the major findings of this study are presented. Finally, the conclusions are provided in the last section.

STUDY AREA AND DATA USED

A total of 226 contiguous sub-basins that cover the entire Indian mainland are selected as individual study areas. These sub-basins are from 21 groups, including major river basins, as shown in Figure 1. The area of these sub-basins ranges from 111 to 91,268 km^2, with the circularity ratio ranging from 0.068 to 0.642. Most of the sub-basins receive the maximum amount of rainfall during the monsoon months (June–September); however, the climatology of these sub-basins is diverse. The daily precipitation, maximum and minimum air temperature, and total soil moisture content obtained from six CORDEX models (Table 1) are regridded to common 0.5° (latitude) × 0.5° (longitude) for the period 1961–2100 (1961–2005 is termed the historical period, and future simulations for two representative concentration pathways (RCP 8.5 and RCP 4.5) are available for the period 2006–2100). These CORDEX simulated variables are then bias-corrected using the observed precipitation obtained from the India Meteorological Department (Pai *et al.* 2014), air temperature and soil moisture reanalysis data obtained from the European Centre for Medium-Range Weather Forecasts Re-Analysis-5 (ERA5) (Hersbach 2016), respectively. The ERA5 data are available from 1979 onward. Hence, limited by the availability of ERA5 data, the bias correction

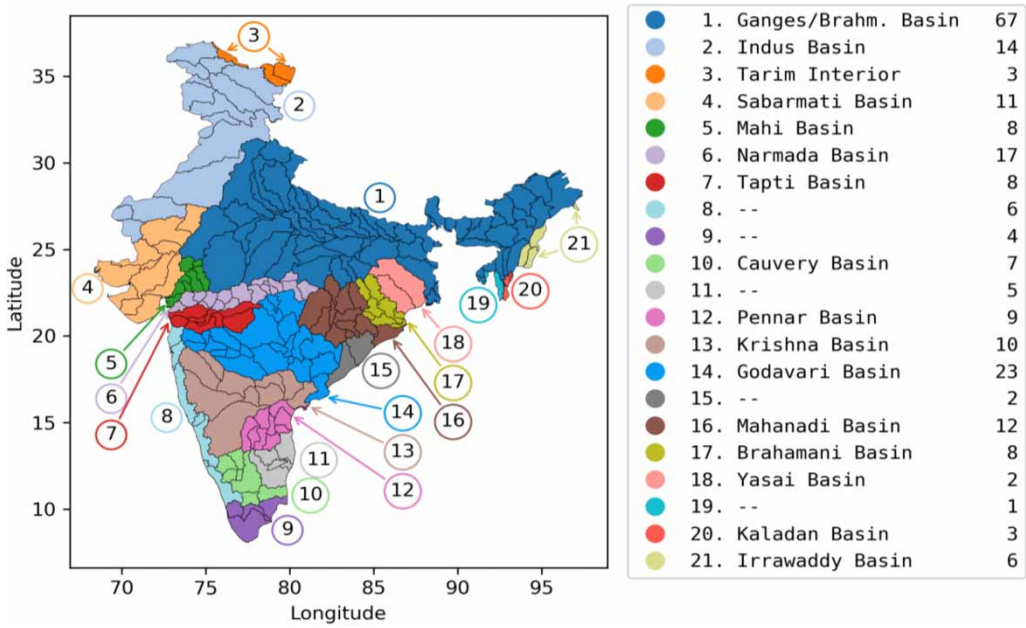

Figure 1 | Sub-basins and major basins (and other groups of sub-basins) of India. In the legend, the major basin name is provided along with the number of sub-basins falling inside the major basin (right column). Some coastal groups of sub-basins like 8, 9, and others (marked as --) are not part of any major basin as they directly flow into the sea in the form of multiple small channels.

Table 1 | Details of different CORDEX simulation outputs used in this study

S. No.	RCM Used	GCM forcing	Spatial resolution	Institute
1	REMO2009	MPI-ESM-LR	0.5° latitude × 0.5° longitude	MPI-CSC
2	RegCM4	CNRM-CM5	50 km × 50 km	IITM
3	RegCM4	CSIRO-Mk3.6.0	50 km × 50 km	IITM
4	RegCM4	IPSL-CM5A-LR	50 km × 50 km	IITM
5	RegCM4	MPI-ESM-MR	50 km × 50 km	IITM
6	RegCM4	GFDL-ESM2M	50 km × 50 km	IITM

All models provide simulations for both RCP 4.5 and RCP 8.5 scenarios.
MPI-CSC, Climate Service Center, Max Planck Institute for Meteorology; IITM, Indian Institute of Tropical Meteorology.

is carried out using the data for the period 1979–1995, and the performance of bias correction is tested for the period 1996–2005. The calibrated bias-correction technique is then used to bias-correct the future CORDEX simulations (2006–2100) for both RCPs. For modeling the temporal consequences of predictor drought indices (either of the SPI or SPEI), the data from the period 1979–1999 are used for calibrating the model performance. The rest of the historical period (i.e., 2000–2005) is used for testing the model performance. The calibrated model is used for predicting the status of agricultural drought for the future period (2006–2100) for both RCPs.

METHODOLOGY

The methodological overview is shown in Figure 2. The methodology can be divided into five modules: (i) bias-correction of precipitation, temperature, and soil moisture obtained from CORDEX simulation and estimation of

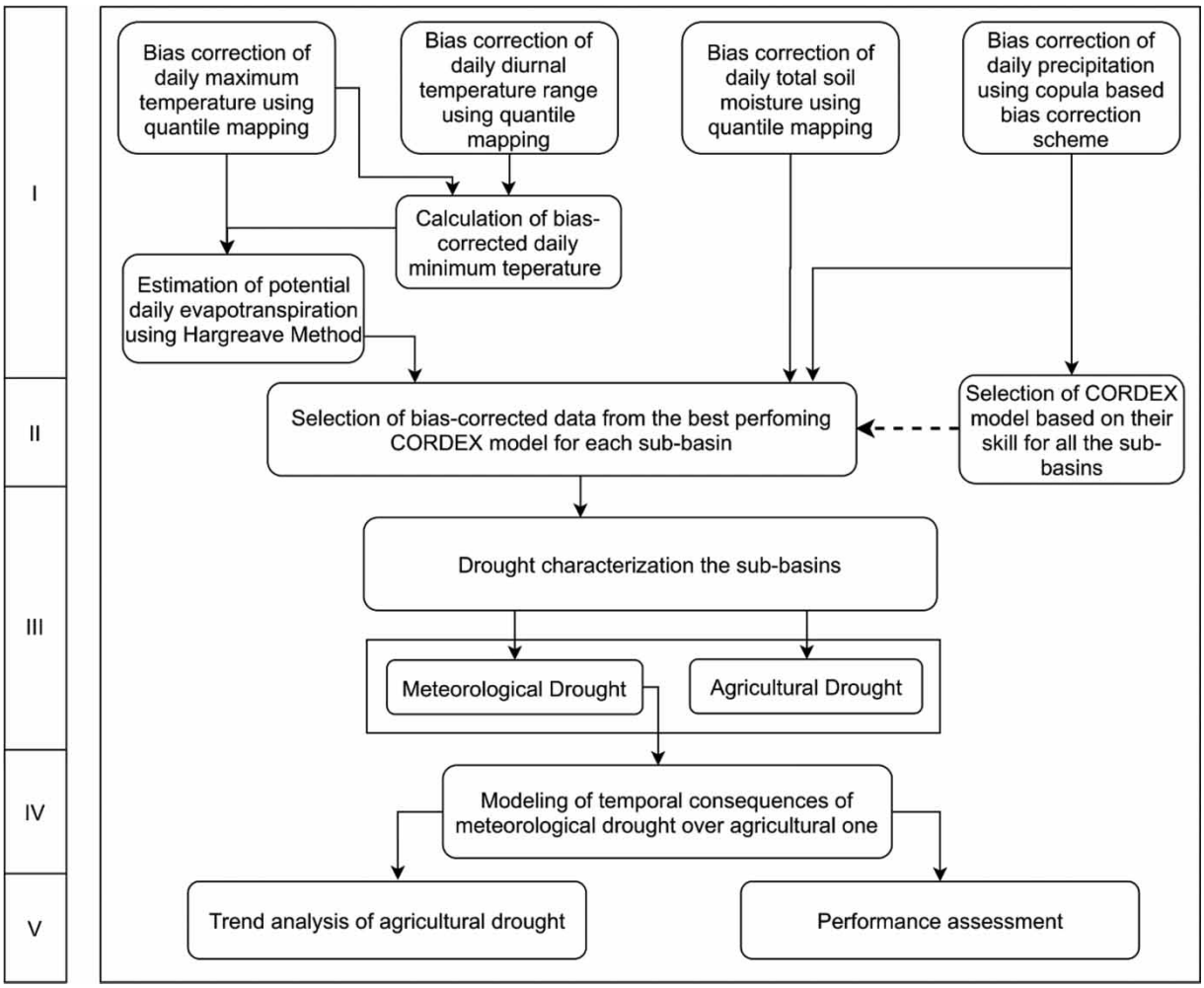

Figure 2 | Methodological overview. The left margin shows the different modules of the methodology. The solid and dashed arrow lines show the transfer of data and information (ranking of CORDEX models in this case), respectively, between the operations.

evapotranspiration, (ii) selection of the best performing CORDEX model based on its skill to simulate sub-basin precipitation, (iii) drought characterization using the bias-corrected data from the selected model, (iv) modeling of the temporal consequences of meteorological drought over agricultural drought, and (v) frequency and trend analysis of agricultural drought. It should be noted that a major issue with assessing the future status of agricultural drought is the comparatively high uncertainty associated with soil moisture estimates from the GCM/Regional Climate Model (RCM) (Stevens & Bony 2013; Lauer *et al.* 2017; Sharma *et al.* 2018). In this study, agricultural drought is modeled using bias-corrected soil moisture values from the best performing CORDEX model and the concept of the temporal consequences of meteorological drought (obtained from the meteorological variables with comparatively less uncertainty). Different modules of the methodology are discussed in subsequent subsections.

Bias-correction of CORDEX simulation outputs

Future CORDEX simulated precipitation, soil moisture, and near-surface air temperature are used for characterizing meteorological drought, agricultural drought, and estimation of evapotranspiration, respectively. However, the CORDEX simulations may have bias, and the bias characteristics are not expected to be the same/similar for all variables. For instance, the bias characteristics differ from

the variable(s) with many zero values (such as precipitation) to other variables, such as air temperature and soil moisture, that do not have any specific repetitive value. Hence, a suitable bias-correction approach should be utilized depending upon the variable being bias-corrected.

In the case of precipitation, a copula-based bias-correction approach (Maity *et al.* 2019) is applied. The copula-based bias-correction technique is used due to its benefit in the context of zero-inflated precipitation series. This method does not suffer from some of the shortcomings faced by many of the existing bias-correction techniques, such as empirical- or distribution-based Quantile Mapping (QM) and linear or nonlinear transfer function. Examples of such shortcomings include correcting bias in the first- or second-order statistics only, ignoring zero values, unable to preserve the shape of the probability distribution of the precipitation including zero values, etc. The copula-based bias-correction approach was formulated to achieve better results than other methods, as this approach properly considers the significant percentage of zero values. The bias-correction approach employs bivariate-copula functions for modeling the relationship between observed and CORDEX simulated precipitation with proper consideration to zero precipitation values.

QM is used for correcting bias for variables like air temperature and soil moisture. This mapping technique is used for bias-correcting the variables not having many zero values, because it considers all statistical moments in simulated data in bias correction (Thrasher *et al.* 2012), and hence, it gives satisfactory results at reasonable computational requirements compared with other alternatives. In the case of daily near-surface air temperature records, the maximum air temperature and diurnal temperature range (the difference of the daily maximum and minimum air temperature) are bias-corrected using QM. The daily minimum air temperature is obtained as the difference of the bias-corrected daily maximum air temperature and the bias-corrected diurnal temperature range. This scheme of bias-correcting daily minimum air temperature ensures that the daily minimum air temperature is always less than the daily maximum air temperature and is recommended (Thrasher *et al.* 2012). QM corrects the bias based on the assumption of stationarity of the probability distribution of the observed and simulated values of the same variable in the future. During the calibration of the QM method, the cumulative probability function for both observed data and simulated values is ascertained, which is deemed the same for the future period. For bias-correcting a simulated value from the future, the value is converted to nonexceeding quantile (or reduced variate) using the corresponding calibrated distribution. The bias correction is then carried out by using this reduced variate against the calibrated distribution of the observed data. Hence, the bias-corrected value ($\tilde{S}$) for a simulated variable (say S) using QM is expressed as follows:

$$\tilde{S} = F_o^{-1}(F_s(S)) \tag{1}$$

where F_o and F_s are the calibrated cumulative distribution functions for the observed data and simulated values, respectively.

Selection of the best performing CORDEX model

Bias correction cannot be considered as a solution to inadequate modeling of climatic systems by climate models (Maraun *et al.* 2017). For instance, many RCMs (including CORDEX models) are not able to reproduce seasonality well, and some RCM models also show a drizzle effect (i.e., very low rainfall simulation for dry days; Schmidli *et al.* 2006; Fowler *et al.* 2007; Christensen *et al.* 2008; Teutschbein & Seibert 2010; Elía *et al.* 2017). Hence, even after the bias correction, not all CORDEX simulations have the same skill. Before hydrological modeling, an analysis of the relative skill of the CORDEX model and the selection of the best model based on the skill can be helpful. The relative skills of multiple CORDEX models are quantified by using the Multi-Criteria Decision-Making (MCDM) methods of outranking nature, such as Compromise Programming (CP) (Kumar 2010; Raju *et al.* 2017) and Preference Ranking Organization METHod of Enrichment Evaluation-2 (PROMETHEE-2; Brans *et al.* 1986; Kumar 2010; Pomerol & Barba-Romero 2012; Raju & Kumar 2014). For the application of these MCDM methods, multiple performance statistics are calculated for historical CORDEX simulations by comparing them with the observed data. The MCDM methods utilize these performance statistics for making decisions.

Compromise programming

CP ranks different CORDEX simulations based on the distance of their performance statistics from the best possible values of performance statistics. The distance measure for a CORDEX simulation is defined as follows:

$$L_p(m) = \left[\sum_{i=1}^{s} w_i^p |f_i^* - f_i(m)|^p\right]^{\frac{1}{p}} \quad (2)$$

where subscript $i \in \{1, 2, \ldots, s\}$ and s is the total number of performance statistics. The f_i^* and w_i are the best value and weight of ith performance statistics, respectively; $f_i(m)$ and $L_p(m)$ are the values of ith performance statistics and the distance measure for mth CORDEX simulation with parameter p. In this study, $p = 2$, and hence, L_2 distance measure (or the weighted Euclidean distance) has been used. The weight for performance statistics is estimated using the entropy method, as discussed in the subsequent section.

Preference Ranking Organization METHod of Enrichment Evaluation-2

PROMETHEE-2 ranks different alternatives (CORDEX simulations in this study) based on the preference/criterion function. It has been employed to rank GCMs (Raju & Kumar 2014). The preference function (denoted by $P_i(m_j, m_k)$) utilizes the pairwise difference in the ith performance measure (denoted by $d_i(m_j, m_k)$) between two CORDEX simulations (denoted by m_j and m_k). There are six types of preference functions, namely, (i) usual criterion, (ii) quasi criterion, (iii) linear preference with no indifferent area, (iv) linear preference with indifferent area, (v) level criterion, and (vi) Gaussian criterion. In this study, the usual criterion function is utilized to rank the CORDEX simulation. Using the usual criterion function, the preference function for different performance measures and pairs of CORDEX models are expressed as follows:

$$P_i(m_j, m_k) = (d_i(m_j, m_k) > 0) \quad (3)$$

The preference functions for different performance measures are weighted-averaged to obtain the multicriteria preference index for a pair of CORDEX models, $I(m_j, m_k)$,

$$I(m_j, m_k) = \frac{\sum_{i=1}^{s} w_i P_i(m_j, m_k)}{\sum_{i=1}^{s} w_i} \quad (4)$$

where w_i is the weight for the ith performance measure, and s is the number of performance measures used. The weight for different performance measures can be estimated using their entropy, as discussed in the next section. It should be noted that the model m_j is better than m_k pairwise if $I(m_j, m_k) > I(m_k, m_j)$. In the case of multiple CORDEX models, the mean net difference of $I(m_j, m_k)$ and $I(m_k, m_j)$, known as the outranking index (denoted by $\phi(m_j)$ for the jth model), is used for ranking.

$$\phi(m_j) = \frac{\sum_{k=1;k\neq j}^{N} (I(m_j, m_k) - I(m_k, m_j))}{N-1} \quad \text{for } j \in \{1, 2, \ldots, N\} \quad (5)$$

where N is the total number of CORDEX simulations being compared. The CORDEX simulation having the highest $\phi(m_j)$ is considered to be the best among the options.

Entropy method for weighting performance statistics

In the MCDM methods for ranking CORDEX simulation, the relative weights for different performance measures are calculated by the entropy of performance measures (i.e., the amount of information present in the performance measures). Before calculating the entropy, the performance measures are normalized using their sum to reduce the effect of scale, if any. If f_{ij} denotes the value of the ith performance measure for the jth model, then the normalized performance measure for the model is expressed as follows:

$$f'_{ij} = \frac{f_{ij}}{\sum_{j=1}^{N} f_{ij}} \quad (6)$$

where N is the number of CORDEX simulations. The normalized values of the performance measures lie between 0

and 1. It should be noted that the entropy can be calculated only for the performance measures that are positive or zero. Based on this criterion, four performance measures are selected to rank the CORDEX simulations on the basis of their skill, namely, R^2, TSS, MAE, and uRMSE. All of these performance measures are positive and lower bounded by 0. The R^2 is the fraction of variance of the observed variable explained by using the modeled/simulated variable. For the best performing model, R^2 will be 1. TSS was proposed by Taylor (2001), with an assumption that a skillful model should be able to accurately simulate both the amplitude and the pattern of variability. Hence, TSS considers both the linear correlation and the ratio of variance and is expressed as follows:

$$\mathrm{TSS} = \frac{4(1+r^4)}{(\hat{\sigma}_f + 1/\hat{\sigma}_f)^2(1+r_0)^4} \tag{7}$$

where r and r_0 are the Pearson's Correlation Coefficient and the maximum Pearson's Correlation Coefficient possible, given the climatic variation between the modeled/simulated variable and the observations. $\hat{\sigma}_f$ represents the ratio of the standard deviation of the modeled and observed values of the variable. The TSS ranges between 0 and 1 (the best possible model). The uRMSE is the Root Mean Square Error (RMSE) between the 'deviation from respective mean' series of the observed and modeled/simulated variable. The MAE is the average of absolute deviation between the observed and modeled/simulated variable. The measures of error, both uRMSE and MAE, are lower bounded by zero (the best performing model) and have no upper bound.

Using the normalized performance measures, the entropy of the ith performance measure (denoted as E_i) is calculated as (notations explained earlier):

$$E_i = -\frac{1}{\ln(N)} \sum_{j=1}^{N} f'_{ij} \ln(f'_{ij}) \tag{8}$$

For a performance measure with high entropy, the uncertainty is also high, and it should have less weightage. The degree of diversification of the information provided by the ith performance measure (D_i) is calculated as $(1 - E_i)$. Hence, for a performance measure with high entropy, the degree of diversification of information will be low. The weight of the ith performance measure is expressed as:

$$w_i = \frac{D_i}{\sum_{i}^{s} D_i} \tag{9}$$

where s is the total number of performance measures used. High weightage, as calculated above, means low relative uncertainty, and hence, higher importance (as compared with others) for the performance measure.

Drought characterization using bias-corrected CORDEX output

Drought can be characterized on a long- or short-temporal scale. As the primary objective of this study is to predict the status of agricultural drought, a short-term drought characterization for the 3-month averaging period is carried out. This short duration is well-suited for analyzing agricultural drought as crops are planted and rotated seasonally (~3 months in India). The drought is characterized using the standardized index. In this study, the SPI and SPEI are used for meteorological drought quantification. Similarly, the SSMI is used for characterizing agricultural drought. These standardized indices are mathematically consistent with each other, which is desirable in a study involving their inter-relation. The methodology for calculating the SPI and SSMI is discussed in Maity *et al.* (2016b).

The SPEI is the standardized index similar to the SPI, with the difference that instead of monthly precipitation, monthly water deficit or climatic water balance is used for calculating the index (Vicente-Serrano *et al.* 2010; Beguería *et al.* 2014). Monthly climatic water balance is the difference between monthly precipitation and potential evapotranspiration (PET) (i.e., the difference between available water and atmospheric evaporation demand); hence, it should be a more reliable measure for drought. However, the use of monthly climatic water balance gives rise to an additional issue as values less than zero are possible. Hence, a three-parameter log-logistic distribution is used instead of a two-parameter gamma distribution (as in the case of the SPI). As the SPEI is derived from monthly climatic water balance, it is a more desirable drought index

in a warming world (Vicente-Serrano *et al.* 2010; Beguería *et al.* 2014; Hernandez & Uddameri 2014; Liu *et al.* 2016).

Multiple methodologies exist for estimating PET, such as Penman–Monteith (Liu *et al.* 2016; Feng *et al.* 2017), Thornthwaite (Hernandez & Uddameri 2014; Feng *et al.* 2017), Hargreaves (Hargreaves 1994; Oguntunde *et al.* 2017; Spinoni *et al.* 2018), Artificial Intelligence-based models (Ghorbani *et al.* 2018) and others. Of these methods, the Penman–Monteith method is considered the most accurate; however, this method is data-intensive (Bisht *et al.* 2019). The Thornthwaite method is considered inferior to both the Penman–Monteith and Hargreaves methods (Bandyopadhyay *et al.* 2012), and it requires monthly mean temperature for estimating PET. The Hargreaves method utilizes the daily maximum, minimum, and average near-surface air temperature, and solar declination for the area to estimate PET. In this study, the PET (say ET_o in mm/day) is estimated using the Hargreaves method as follows:

$$ET_o = 0.0023 \times R_a (T_{avg} + 17.8)\sqrt{(T_{max} - T_{min})} \tag{10}$$

where T_{max}, T_{min}, and T_{avg} are the maximum, minimum, and average daily air temperature, respectively in °C; R_a is extra-terrestrial radiation (radiation received on the top of the atmosphere) expressed in mm/day. R_a at a location with latitude l (in radian) is estimated as follows:

$$\begin{aligned} R_a &= 0.408\frac{118 r_d}{\pi}[\omega \sin(l)\sin(S_d) + \cos(l)\cos(S_d)\sin(\omega)] \\ \omega &= \arccos(-\tan(S_d)\tan(l)) \\ S_d &= M_a \sin\left(\frac{2\pi}{365}(d - 80)\right) \\ r_d &= 1 + (1/30)\cos\left(\frac{2\pi d}{365}\right) \end{aligned} \tag{11}$$

where S_d, r_d, and M_a are the solar declination in degrees for the dth day of the year, the relative distance between the Earth and the Sun for the dth day of the year, and the mean axial tilt of the Earth (taken as 23.43673°), respectively. It should be noted that the relative temporal estimation of PET is used when it is included in the drought index (SPEI); hence, the method used for the estimation of PET is not crucial (Vicente-Serrano *et al.* 2010, 2014).

Modeling of the temporal consequences of meteorological drought

It is established that droughts translate from one type to another (Maity *et al.* 2016b; Suman & Maity 2016; Shamshirband *et al.* 2020). For instance, meteorological drought (rainfall deficit) may lead to agricultural drought (soil moisture deficit) and further to hydrological drought (stream flow/groundwater/reservoir storage deficit). Secondly, climate models are more efficient in the simulation of primary hydroclimatic variables (e.g., precipitation) as compared with secondary (e.g., soil moisture, stream flow) and tertiary (drought indices) hydroclimatic variables (Moss *et al.* 2010; Stevens & Bony 2013). Thus, it may be beneficial to use the potential of climate models at primary hydroclimatic variables to investigate the change in drought characteristics in the past and future for a better assessment. Thus, temporal consequence or inter-relation between different types of droughts is utilized for making a future assessment of agricultural droughts.

The wavelet-based models for analyzing the temporal consequence of meteorological drought to agricultural and hydrological droughts were developed by Maity *et al.* (2016b). The models linking meteorological drought (characterized by the SPI) to agricultural drought (characterized by the SSMI) are used in this study. It should be noted that these models are framed based on a hypothesis that the inter-relation between drought should be continuous in time, and hence, it should be studied on the constituent frequency or component level of drought indices. Wavelet Transform is used to separate these constituent components of drought indices. Fourier Transform is avoided as it averages out temporal information while identifying the constituent frequencies, which is not desirable in a model assessing temporal consequence on predecessor drought on successor drought. Details of the utilized models are provided in Table 2. First, the series of drought indices are transformed into their constituent wavelet components using Multi-Resolution Stationary Wavelet Transform (MRSWT) up to level 2, resulting in three components for each drought index. Next, the inter-relation between drought indices is modeled on the component level. For instance, models 1 and 2 predict the SSMI series using Multiple Linear Regression (MLR) of the wavelet components of predecessor drought indices (the SPI and/or

Table 2 | Models for the temporal consequences of meteorological drought on agricultural drought

S. No.	Model description
1	$\mathrm{SSMI}(t) = f\begin{pmatrix} \mathrm{SPI}_{a_2}(t-T_1), \mathrm{SPI}_{d_2}(t-T_1), \mathrm{SPI}_{d_1}(t-T_1) \\ \mathrm{SPI}_{a_2}(t-T_2), \mathrm{SPI}_{d_2}(t-T_2), \mathrm{SPI}_{d_1}(t-T_2) \end{pmatrix}$
2	$\mathrm{SSMI}(t) = f\begin{pmatrix} \mathrm{SPI}_{a_2}(t-T_1), \mathrm{SPI}_{d_2}(t-T_1), \mathrm{SPI}_{d_1}(t-T_1) \\ \mathrm{SPI}_{a_2}(t-T_2), \mathrm{SPI}_{d_2}(t-T_2), \mathrm{SPI}_{d_1}(t-T_2) \\ \mathrm{SSMI}_{a_2}(t-T_1), \mathrm{SSMI}_{d_2}(t-T_1), \mathrm{SSMI}_{d_1}(t-T_1) \end{pmatrix}$
3	$\mathrm{SSMI}_C(t) = f\begin{pmatrix} \mathrm{SPI}_{a_2}(t-T_1), \mathrm{SPI}_{d_2}(t-T_1), \mathrm{SPI}_{d_1}(t-T_1) \\ \mathrm{SPI}_{a_2}(t-T_2), \mathrm{SPI}_{d_2}(t-T_2), \mathrm{SPI}_{d_1}(t-T_2) \\ \mathrm{SSMI}_{a_2}(t-T_1), \mathrm{SSMI}_{d_2}(t-T_1), \mathrm{SSMI}_{d_1}(t-T_1) \end{pmatrix}$ for $C \in \{d_1, d_2, a_2\}$
	$\mathrm{SSMI}(t) = g(\mathrm{SSMI}_{d_1}, \mathrm{SSMI}_{d_2}, \mathrm{SSMI}_{a_2})$

The symbols f and g represent Multiple Linear Regression (MLR) and inverse wavelet functions, respectively. $T_2 = T_1 + 1$; $T_1 = 2^l$, where l is highest MRSWT level (i.e., 2 in this study).

SSMI) time series. Model 1 uses the information of the SPI only for SSMI prediction, and it assumes that the memory in the SSMI is not significant. However, model 2 additionally uses the memory of the SSMI while predicting the SSMI. Model 3 predicts the wavelet components of the SSMI series using the wavelet components of the SPI and SSMI time series, which are transformed into the SSMI series using inverse wavelet transform. These models were found to capture the temporal consequence of drought satisfactorily in the Upper Mahanadi Basin (Maity *et al.* 2016b). The same models are also run with the SPEI as input for assessing its temporal consequences, which helps in assessing the relative performance of the SPEI compared with SPI in predicting the SSMI.

The models are run using two validation schemes (i.e., validation schemes I and II; Figure 3). Under validation scheme I (also known as a fixed development and testing period), the model is calibrated once over the development period and the SSMI is predicted over the testing period using the same calibrated model parameters. However, in the case of validation scheme II (also known as a moving window approach), the model is calibrated on the development period, and using the calibrated parameters, a single value after the development period is predicted. In the next iteration, the development period window is moved forward by one time step, and the process of model calibration on the shifted development period followed by the prediction of the single value after the development period is repeated. The shifting of the development period continues until prediction for all of the time steps is complete. Due to the shifting window and repeated calibrations, validation scheme II is more suitable for the cases in which the relationship is expected to change with time.

The performance of the models is evaluated using the Pearson's Correlation Coefficient (r), Refined Index of Agreement (Dr), Nash–Sutcliffe Efficiency (NSE), and uRMSE (Krause *et al.* 2005; Willmott *et al.* 2012; Maity *et al.* 2019). The first two performance measures (r and Dr) measure the association between the predicted and the observed SSMI. The maximum value of these performance measures is 1 for the best performing model. The NSE and uRMSE are dependent upon the error/deviation between the predicted and the observed SSMI. An error variance equal to zero (the best performing model) will result in the NSE being equal to 1. For the positive error variance, the NSE < 1. In the case of the uRMSE (i.e., the RMSE between the 'deviation from mean' series of the predicted and observed SSMI), the best performing model is expected to have a uRMSE of 0.

$$r = \frac{cov(\hat{Y},\ Y)}{S_{\hat{Y}} S_Y} \tag{12}$$

$$Dr_{frac} = \frac{\sum |\hat{Y} - Y|}{2\sum |Y - \bar{Y}|}$$
$$Dr = \begin{cases} 1 - Dr_{frac} & \text{for } Dr_{frac} \le 1 \\ \dfrac{1}{Dr_{frac}} - 1 & \text{for } Dr_{frac} > 1 \end{cases} \tag{13}$$

$$\mathrm{NSE} = 1 - \frac{\sum (\hat{Y} - Y)^2}{\sum (Y - \bar{Y})^2} \tag{14}$$

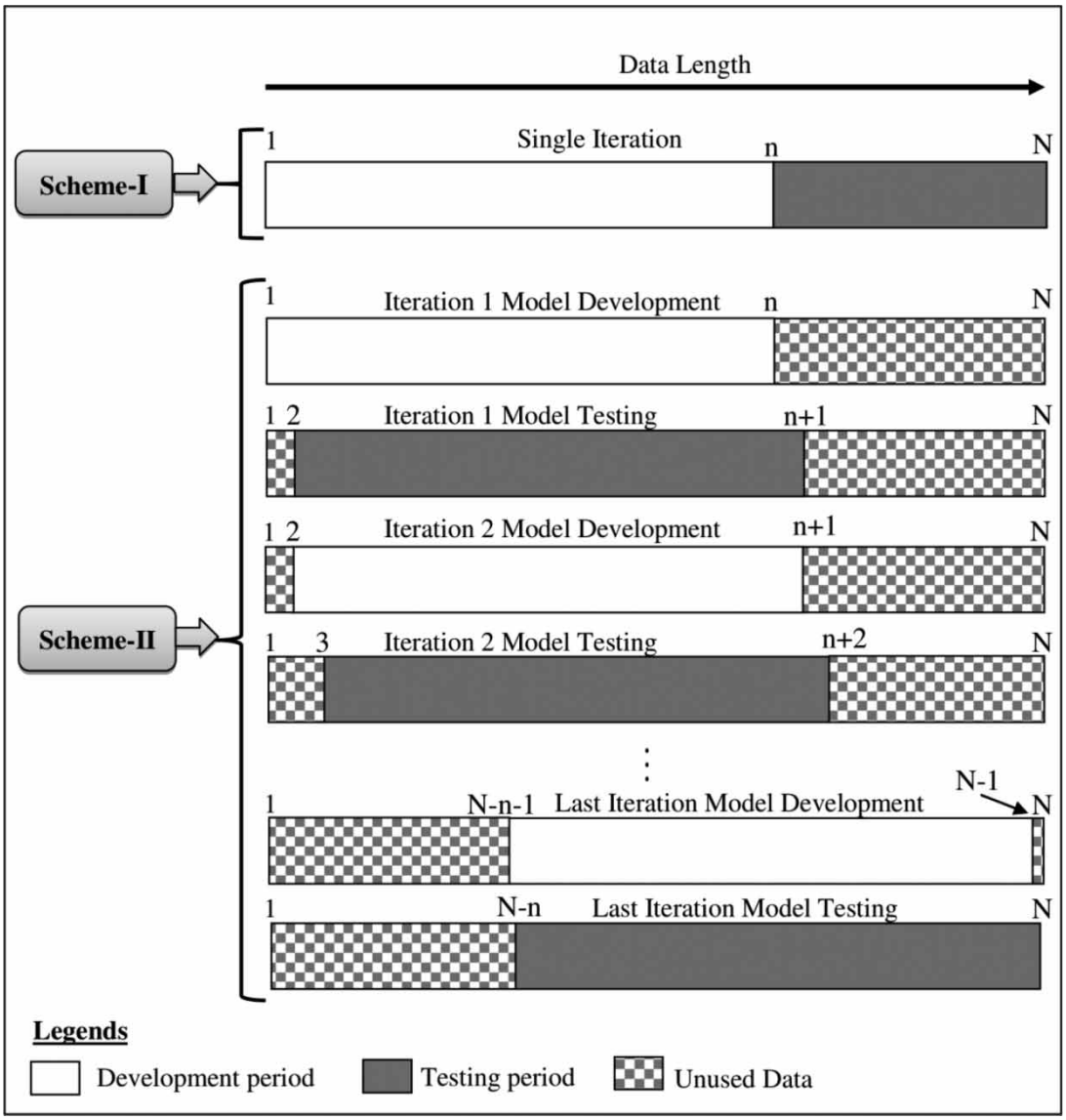

Figure 3 | Schematic diagram of two types of validation schemes. In scheme II, at any model testing iteration, only the last value is recorded for performance assessment, as the other parts of the testing period overlap the model development period of the same iteration (*Source*: Maity *et al.* (2016b)).

$$\text{uRMSE} = \sqrt{\frac{\sum[(Y-\bar{Y})-(\hat{Y}-\overline{\hat{Y}})]^2}{n}} \quad (15)$$

where Y and $\hat{Y}$ represent the observed and predicted SSMI series. Similarly, $\bar{Y}$ and $\overline{\hat{Y}}$ represent the mean of the observed and predicted SSMI series. S_Y, $S_{\hat{Y}}$, and $cov(\hat{Y}, Y)$ are the standard deviation of the observed SSMI, the standard deviation of the predicted SSMI, and the covariance of the observed and predicted SSMI, respectively.

RESULTS AND DISCUSSION

Bias-correction of CORDEX simulation and their skill-based selection

As stated earlier, the daily precipitation, being a zero-inflated variable, is bias-corrected using the copula-based bias-correction scheme (Maity *et al.* 2019). Other variables, i.e., maximum daily temperature, diurnal temperature range, and daily total soil moisture are bias-corrected using

the QM method. It should be noted that the bias-correction of precipitation was satisfactory (Maity *et al.* 2019). The performance for the bias-correction of maximum temperature during the testing period is shown in Figure 4. It can be observed from the figure that the spatial distribution of QM Corrected (QMC) values matches better than that of the observed mean daily maximum temperature for a month. Across the months, the correspondence between

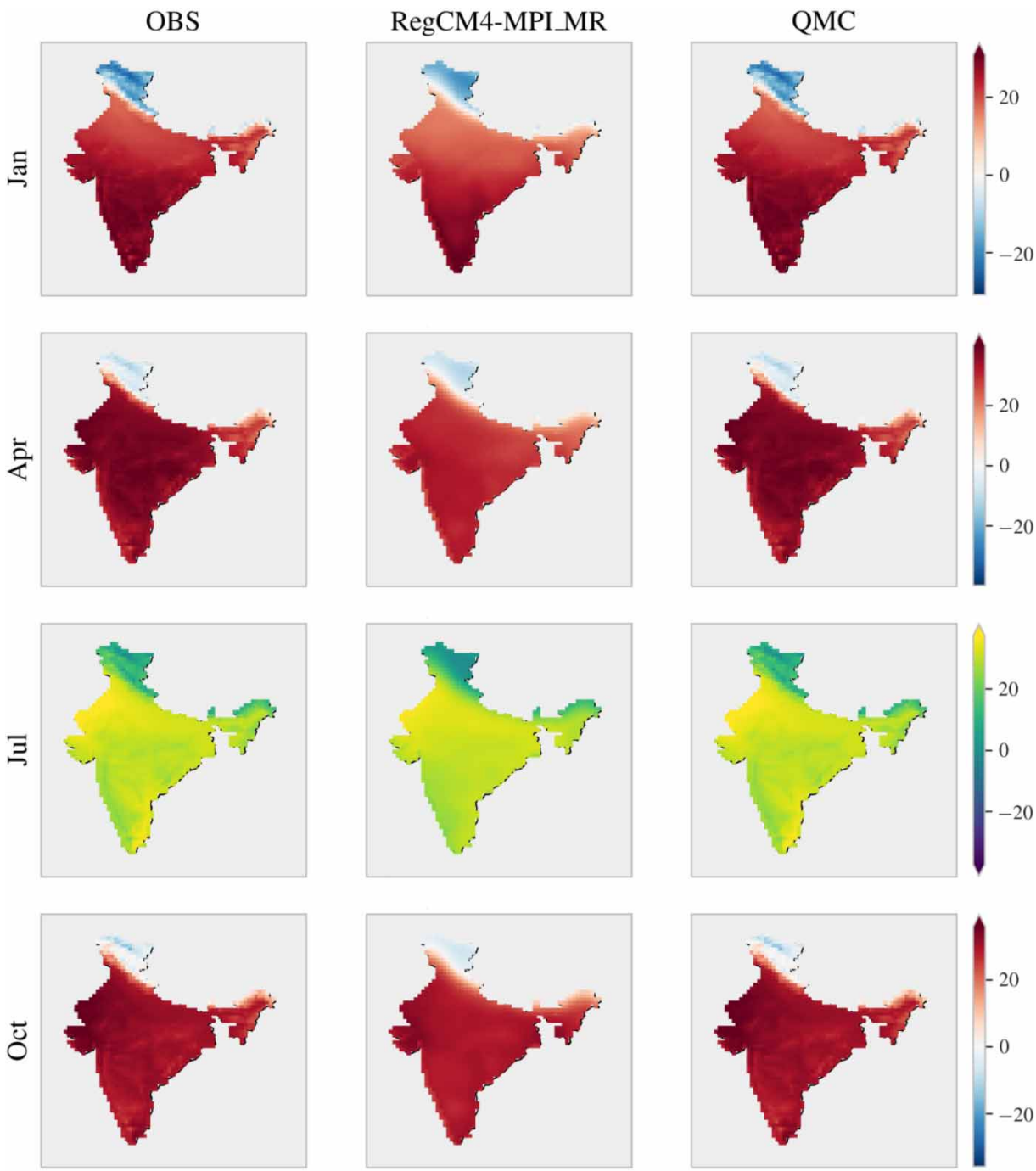

Figure 4 | Spatio-temporal comparison of bias-corrected monthly mean daily maximum near-surface air temperature (QMC) with the corresponding observed (OBS) values and CORDEX simulation (second column) for selected months during the period 1996–2005. The results are shown for the RegCM4 RCM model forced by MPI-ESM-MR GCM.

the QMC and observed data is also better than the correspondence between the CORDEX simulation and observed data. The better spatio-temporal correspondence with the observed data suggests the efficacy of QM in reducing bias in the maximum daily temperature. Similar results are obtained for the bias-corrected values of the diurnal temperature range and soil moisture (figures not shown). In general, the QMC values of these variables are better than the original CORDEX simulations for hydrological modeling. From the bias-corrected values of the diurnal temperature range and daily maximum air temperature, the bias-corrected daily minimum air temperature is obtained. From the bias-corrected values of daily maximum and minimum air temperature, the daily PET is estimated by using the Hargreaves formula at each grid point.

Next, the bias-corrected variables are converted to their monthly values by accumulating them across days. The bias-corrected variables including monthly PET are then spatially averaged over each of the sub-basins using the Thiessen polygon method. The effectiveness of the CORDEX model in reproducing seasonality in monthly precipitation series is evaluated using two MCDM methods, namely, CP and PROMETHEE-2. The performance measures used to characterize the skill of different CORDEX models are R^2, TSS, MAE, and uRMSE. The highest-ranked CORDEX model for each of the sub-basins is shown in Figure 5. It should be noted that the rankings of the CORDEX models from both of the MCDM methodologies are not expected to be the same, as the ranking criteria followed are different in the MCDM methodologies. CP compares the performance of the CORDEX models with respect to the best possible performance. However, PROMETHEE-2 with the usual criterion inter-compares the CORDEX models using their performance measures.

Despite the differences in ranking from these methodologies, RegCM4 RCM driven by MPI-ESM-LR and CSIRO-Mk3.6.0 GCMs is found to be the best models for simulating the monthly precipitation in most of the sub-

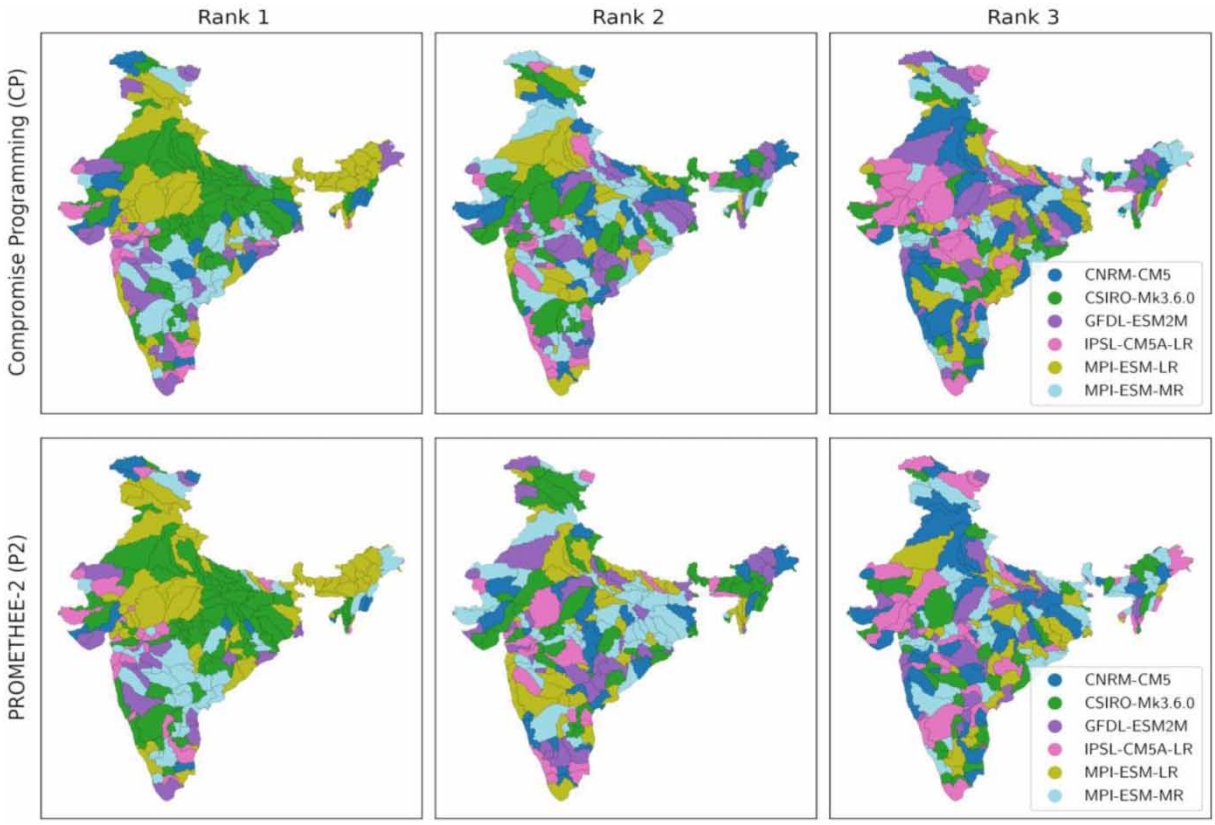

Figure 5 | Top three CORDEX models (rank 1–3) at each sub-basin across the Indian mainland using CP and PROMETHEE-2. The legend shows the driving GCM (Table 2).

basins across north and north-east India. On the other hand, the best selected CORDEX models show more variability for the sub-basins in south India. However, REMO2009 RCM driven by MPI-ESM-MR GCM is found to be the best in most sub-basins of this region. The spatial variation of the ranking of the bias-corrected CORDEX model (along with driving GCM) reveals the effect of differences in modeling parameters and assumptions involved in simulations. Furthermore, it should be noted that despite the better performance of some of the CORDEX models (and their driving GCMs) for the majority of sub-basins, any single CORDEX simulation (and driving GCM) is found incompetent to capture the majority diverse climatology of the Indian mainland. These observations show the importance of performance quantification of GCM/RCM models on a regional scale (in any study involving multiple GCM/RCM simulations) before using them in any further hydrological analysis. The data from the best ranking CORDEX model under either of CP or PROMETHEE-2 are used for studying the temporal consequence of meteorological drought to an agricultural one. It should be noted that the effectiveness of the CORDEX models is not evaluated for other variables, which might have resulted in another set of rankings. The selection of a CORDEX model based on only one variable (i.e., precipitation) ensures that the values of all variables are generated by the same model and, hence, have the same model assumption and parametrization. The translation of meteorological drought to agricultural drought (as discussed in the next section) is then modeled using the bias-corrected values from selected CORDEX models.

Modeling of the temporal consequence of drought

Using the bias-corrected values of monthly precipitation and monthly soil moisture, the SPI and SSMI are calculated at the 3-month running mean of the respective variables. Similarly, the SPEI is calculated using the 3-month running mean of the monthly climatic water balance series (the difference of monthly precipitation and PET series). Wavelet-based models 1–3, as shown in Table 1, are used for predicting the SSMI.

The models are calibrated during the period 1979–1999 and tested during the period 2000–2005. Both validation schemes (I and II) are used in this study. The performance of different models during the development period is shown in Figure 6 for the case when the SPI is used for characterizing metrological drought. From Figure 6, the performance of model 2 is found to be the best among all of the models as evident by the high values of R^2, Dr, NSE and low values of the uRMSE for sub-basins across India. The performance of model 2 is found to be slightly better for the sub-basins in north India on an average as compared with that for the sub-basins in south India. The better performance of models using the past values of the SSMI series (models 2 and 3) as compared with model 1 (which does not use any information from the SSMI series) indicates the high innate memory of soil moisture throughout the sub-basins across India.

The models are also run using the SPEI. Model 2 is found to work marginally better in the case when the SPI is used as input rather than SPEI. This might be due to (i) the warming during the development period might be insignificant (Thomas *et al.* 2015), leading to less evapotranspiration, hence there is no benefit of prediction using the SPEI over SPI (Shamshirband *et al.* 2020); however, it might not be the case in the future as more warming is expected, and the SPEI captures the effect of warming climate better than SPI (Vicente-Serrano *et al.* 2010; Beguería *et al.* 2014; Liu *et al.* 2016) and (ii) the memory of the SSMI is comparatively more significant for modeling the temporal consequence of meteorological drought over agricultural drought. However, in the future, with comparatively warm weather, the near-surface air temperature might affect the SSMI more due to higher evapotranspiration. Hence, the SPEI-based prediction of the SSMI is more desirable for a future period. The performance of model 2 for both validation schemes during the testing period is shown in Figure 7 for the case when the SPI is used for characterizing meteorological drought.

Comparing Figures 6 and 7, the performance of model 2 is found to be comparable during both development and testing periods. This suggests that model 2 is not under- or overfitting. Additionally, it should be noted that the performance across validation schemes (a comparison of Figure 7(a) and 7(b)) suggests no significant advantage for validation scheme II, which was designed to capture any dynamic relationship (if any) during the testing period. Thus, there may not be any significant warming effect during this period. Among all of the model options, model 2 (i.e., the

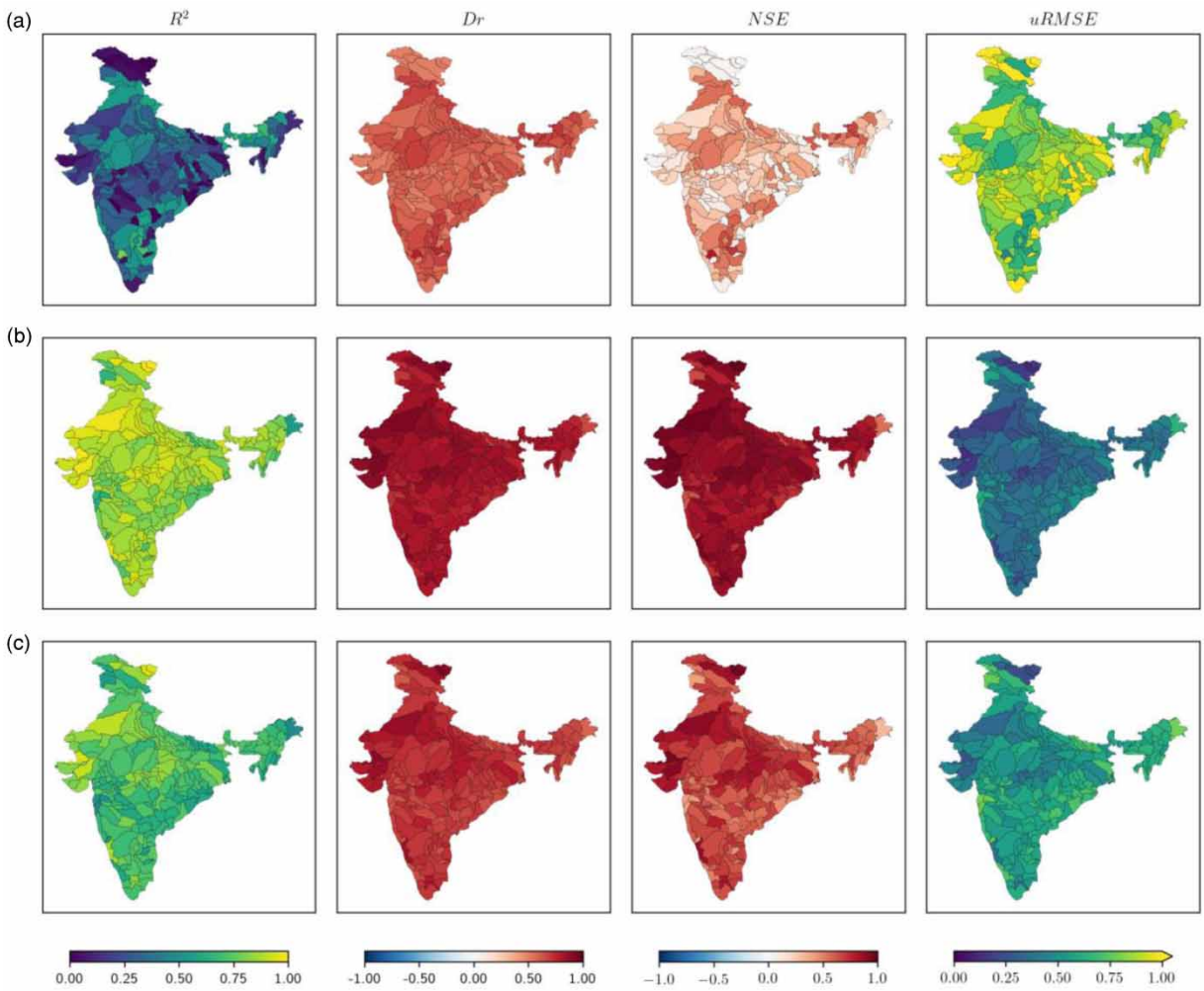

Figure 6 | Performance of (a) model 1, (b) model 2, and (c) model 3 for predicting the SSMI during the development period using validation scheme I. The data for all of the variables are taken from the best (rank = 1) CORDEX simulation selected using CP. Meteorological drought is characterized by the SPI for the analysis.

model relating the SSMI series with the component of predictor drought and the memory of components of the SSMI series) is found to perform the best and, thus, utilized for assessing future agricultural drought.

Analysis of future agricultural drought

The predicted SSMI series for the future period, obtained from a modeling of the temporal consequence of meteorological drought using either of the SPI or SPEI in model 2, are assessed for the state of agricultural drought in sub-basins throughout India. It should be noted that 16 realizations of the SSMI series are obtained – combinations of two choices for each of (i) the validation schemes, (ii) the predecessor meteorological drought indices (the SPI and SPEI), (iii) the best CORDEX model selected on the basis of the CP and PROMETHEE-2 methods, and (iv) RCP scenarios (RCP 4.5 and RCP 8.5). In this section, the results for the SSMI series obtained from the SPEI-based modeling and validation scheme II are discussed. This combination of predecessor drought series and validation scheme is chosen as is expected in warming and changing climates.

A trend analysis of the SSMI series in the future (obtained from the SPEI-based models for validation scheme II; Figure 8) carried out using the Mann–Kendall Test at a 5% level of significance suggests that most of the sub-basins in south India show a more wetting (an increasing trend in the SSMI series) condition. However, most of

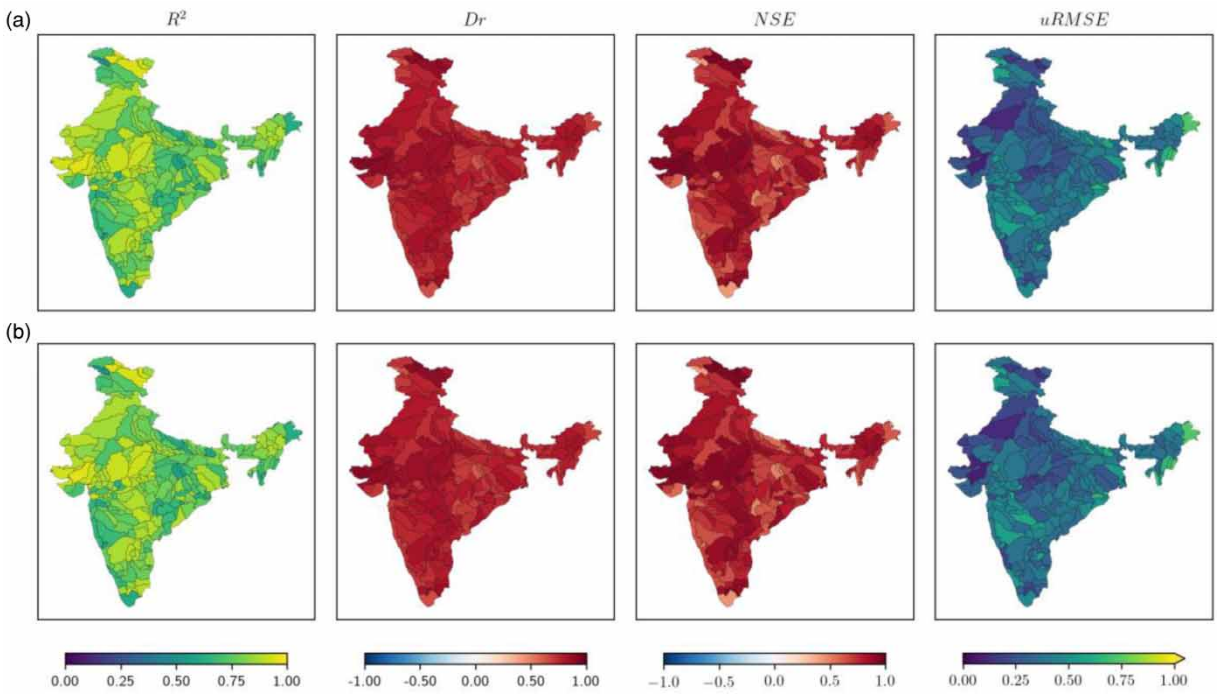

Figure 7 | Performance of model 2 for validation scheme (a) I and (b) II for predicting the SSMI during the testing period. The data for all of the variables are taken from the best (rank = 1) CORDEX simulation selected using . Meteorological drought is characterized by the SPI.

the sub-basins in north, central, and north-east India show the condition of dryness (or a decreasing trend in the SSMI series). This geographically contrasting change in future agricultural drought is in agreement with the expected changes in precipitation in south India as compared with that in north and central India, as suggested by the literature (Suman & Maity 2020). The future period is then separated into three epochs: (i) E1 (2006–2035), (ii) E2 (2036–2070), and (iii) E3 (2071–2100) for the analysis of temporal changes in agricultural drought. This epoch-wise analysis suggests that the trend of the SSMI series in the south Indian sub-basins is expected to become insignificant or dry by the end of this century. The analysis of the trend in the SSMI series predicted using other combinations of the validation scheme and predecessor meteorological drought indices indicates a similar wetting trend in south India and a drying trend in north and central India.

The percentage area under both moderate (SSMI ≤ -1) and extreme (SSMI ≤ -2) agricultural drought conditions for the SSMI index simulated by model 2 using the SPEI and validation scheme II on a monthly scale is expected to increase, as shown in Figure 9. By the end of the century, more than 50% of the Indian mainland is expected to be under moderate agricultural drought for the RCP 8.5 scenario. Similarly, more than 20% of the Indian mainland is expected to be under extreme agricultural drought by the end of the century for the RCP 8.5 scenario. Additionally, it is noticed that CORDEX models selected on the basis of CP show more areas under drought as compared with CORDEX models selected on the basis of PROMETHEE-2.

The distribution of the percentage time for a sub-basin to be under extreme drought conditions for different periods in the future is shown in Figure 10. From the figure, the percentage time for a sub-basin under extreme drought conditions is found to be higher in most of the sub-basins in north, central, and north-east India. Sub-basins in central India are more vulnerable to extreme drought conditions. On the other hand, the vulnerability, and thus, the percentage time under extreme drought conditions is found to be less for most of the sub-basins in south India and for some large sub-basins in western India. Additionally, the epoch-wise analysis shows that the area under drought is increasing with time in the

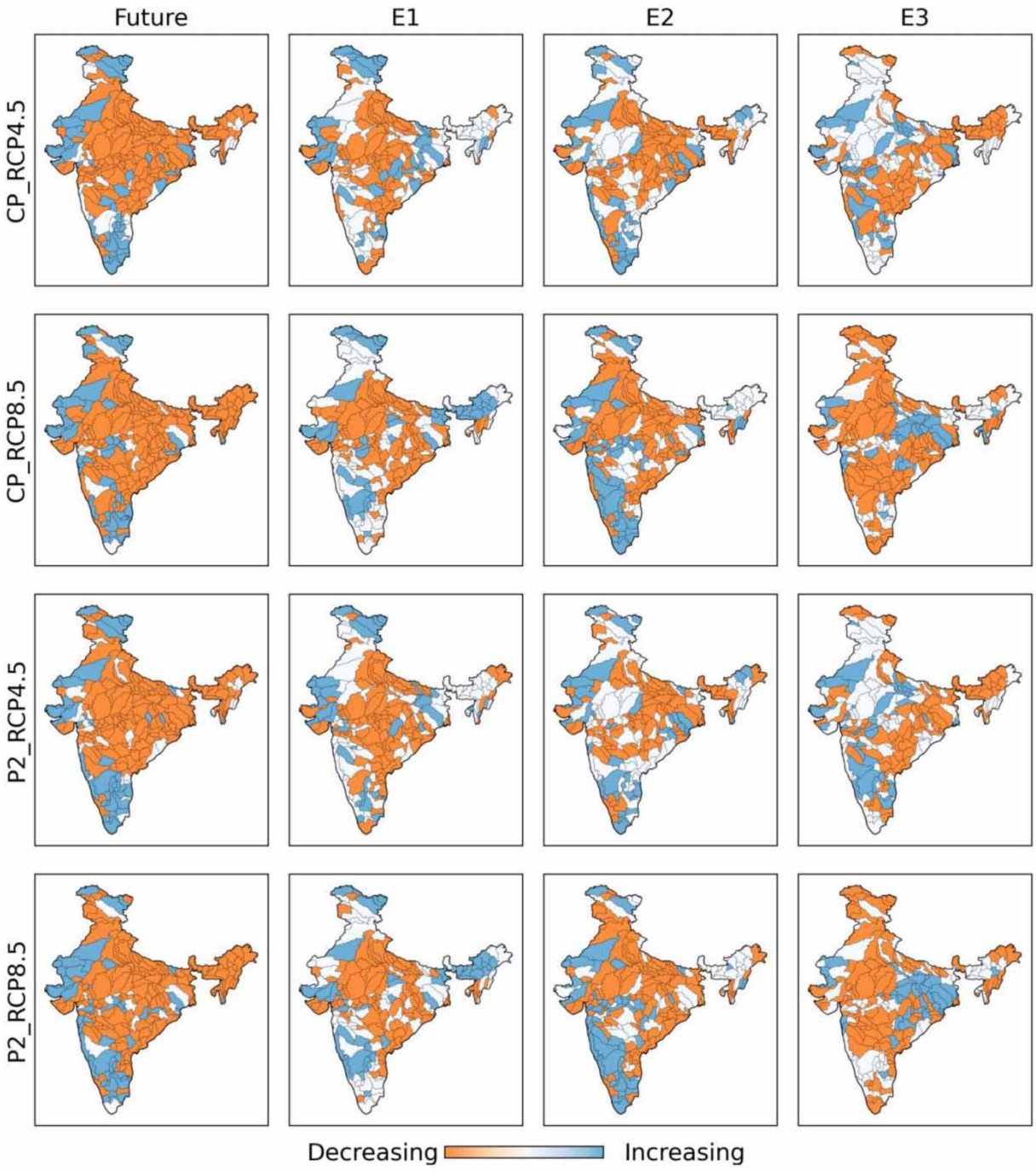

Figure 8 | Trend of the SSMI series for different future periods. The results are provided for model 2 with the SPEI input and validation scheme II. Four columns indicate the entire future period (2006–2100) and three epochs: E1 (2006–2035), E2 (2036–2070), and E3 (2071–2100). The row name shows the method (CP for Compromise Programming and P2 for PROMETHEE-2) and the RCP scenario. The significance of the trend is assessed using the Mann–Kendall Test at a 5% level of significance. Sub-basins showing no significant trend are shown in white patches.

future. It should be noted that most of the sub-basins in the Gangetic plain, a major agricultural region in India, show high vulnerability to extreme drought conditions. Hence, an increased vulnerability of these regions to agricultural drought may have adverse consequences for food security in the Indian sub-continent.

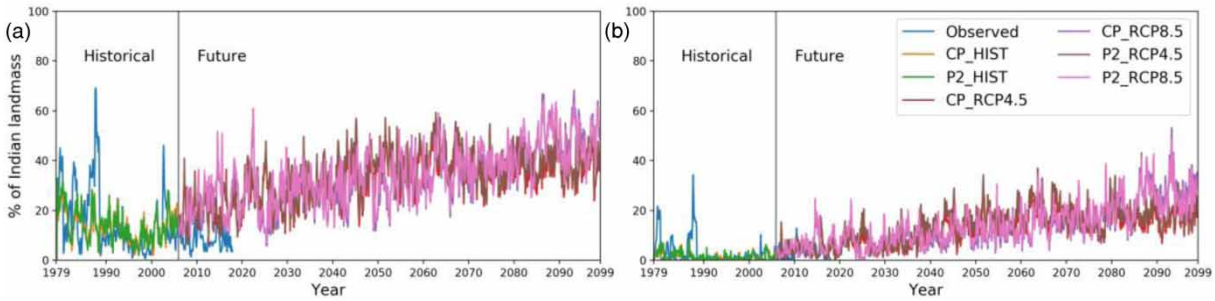

Figure 9 | Monthly series of the percentage area of the Indian mainland under (a) moderate (SSMI ≤ -1)) and (b) extreme (SSMI ≤ -2) agricultural drought conditions. The results are presented for the SSMI predicted by model 2 using the SPEI and validation scheme II. 'Observed' indicates the SSMI calculated using ERA5 Reanalysis data for the time period 1979–2018.

CONCLUSIONS

This study investigates the future status of agricultural drought in 226 sub-basins across India. The translation of meteorological droughts to agricultural droughts is modeled using a recently developed wavelet-based approach. At first, the CORDEX simulation of precipitation, air temperature and others are bias-corrected, and the best performing CORDEX model for simulating precipitation is selected for each sub-basin. Based on the data from the selected CORDEX model, the temporal consequence of predecessor drought to a successor one is modeled. In this study, agricultural drought (characterized by the SSMI) is considered as a successor drought. The temporal consequence modeling is found to perform satisfactorily across India despite varying climatology. Given that the models are not over- or under-fitting, the models are then utilized to estimate the future state of agricultural drought in different sub-basins across India. The major findings regarding the state of future agricultural drought across India are as follows:

(i) The study has identified a geographically contrasting change in the spatial pattern of future agricultural drought over south and north India. Agricultural drought shows an increasing trend in most of the sub-basins in the Indian mainland, except for some of the sub-basins that are situated in south India.
(ii) Sub-basins in north and central India are expected to be vulnerable to frequent agricultural droughts, with the sub-basins in central India expected to be comparatively more vulnerable. However, the vulnerability of sub-basins in south India is found to be comparatively less.
(iii) In general, the percentage area of the Indian mainland under extreme or moderate drought conditions is expected to increase by the end of this century. On average, more than 20% area of the Indian mainland is expected to suffer from extreme agricultural drought conditions (SSMI ≤ -2). Moderate drought conditions (SSMI ≤ -1) will be experienced as much as 50% of the area.
(iv) The percentage time under extreme drought conditions is found to be higher for many sub-basins in north India. It is also noticed that most of the sub-basins in the Gangetic plain exhibit high vulnerability to extreme drought conditions in future. This may have an adverse effect on food production in this region.

Overall, the analysis has identified vulnerable basins across India considering future agricultural drought. It also underlines the geographically contrasting agricultural drought between north and south India. These findings are expected to be highly useful for policymakers for future planning and preparedness in terms of agricultural productivity. Utilizing the temporal consequence of meteorological drought to analyze agricultural drought leads to a reduction in the uncertainty associated with simulated soil moisture; however, simulated precipitation also has uncertainty (though less than a secondary variable like soil moisture). As a way forward, it should be noted that this study is carried out with CORDEX simulations driven

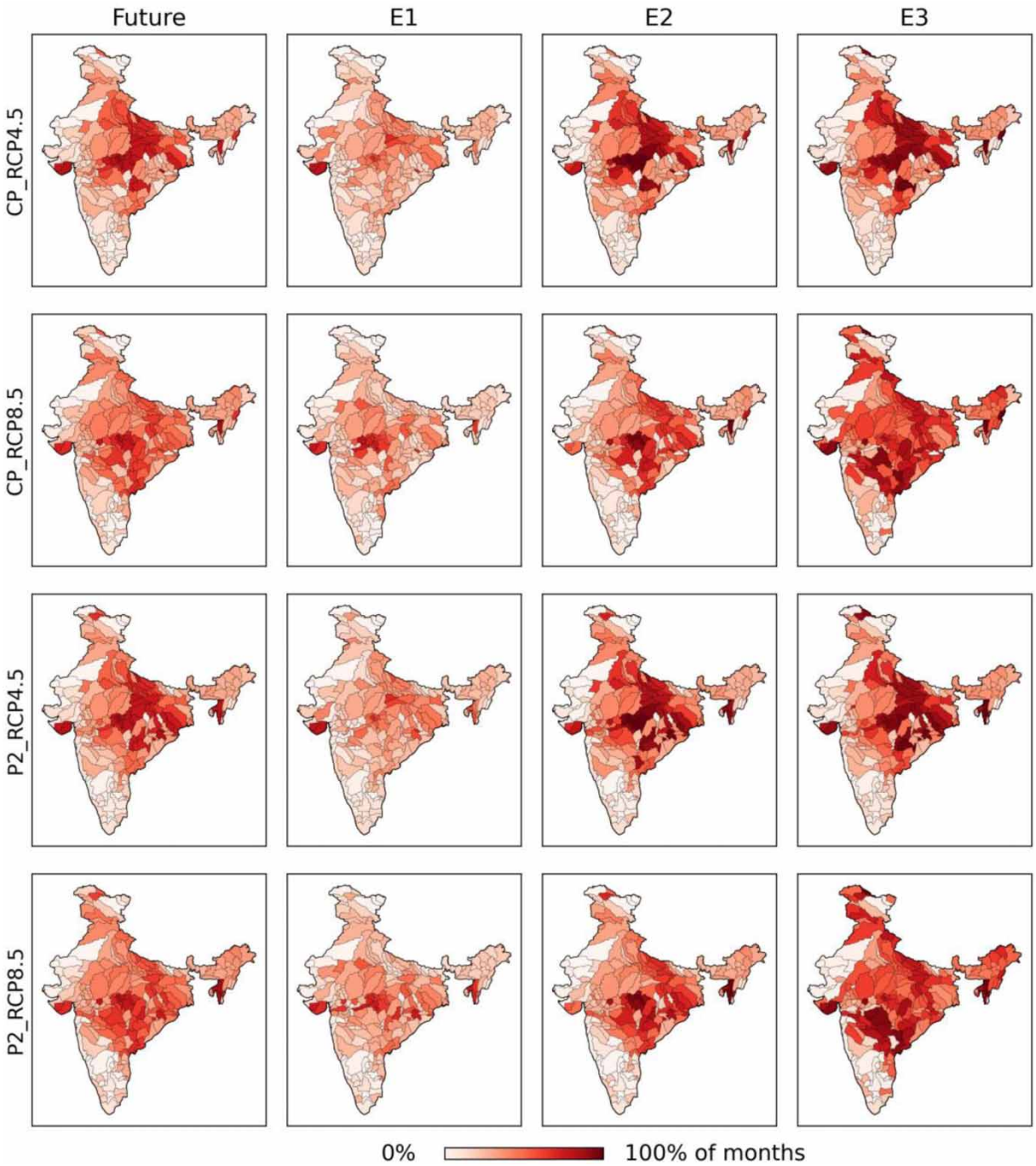

Figure 10 | Sub-basinwise percent time under extreme drought conditions across India for the SSMI predicted by model 2 using the SPEI and validation scheme II.

by the climate models used in Coupled Model Intercomparison Project Phase 5 (CMIP5). With the availability of Coupled Model Intercomparison Project Phase 6 (CMIP6), the analysis can be carried out with improved simulations from CMIP6.

ACKNOWLEDGMENT

This work was partially supported by Department of Science and Technology, Climate Change Programme (SPLICE), Government of India (Ref No. DST/CCP/CoE/79/

2017(G)) through a sponsored project. All authors declare that there is no conflict of interest.

DATA AVAILABILITY STATEMENT

The data used in this study are available from multiple online repositories. The observed daily precipitation records can be obtained from IMD (https://www.imdpune.gov.in/Clim_Pred_LRF_New/Grided_Data_Download.html). Similarly, ERA5 reanalysis data can be downloaded from https://www.ecmwf.int/en/forecasts/datasets/reanalysis-datasets/era5. The CORDEX simulations used in this study were obtained from Earth System Grid Foundation (https://esgf-node.llnl.gov/projects/esgf-llnl/).

REFERENCES

Annamalai, H., Hafner, J., Sooraj, K. & Pillai, P. 2013 Global warming shifts the monsoon circulation, drying South Asia. *Journal of Climate* **26** (9), 2701–2718.

Bandyopadhyay, A., Bhadra, A., Swarnakar, R., Raghuwanshi, N. & Singh, R. 2012 Estimation of reference evapotranspiration using a user-friendly decision support system: DSS_ET. *Agricultural and Forest Meteorology* **154**, 19–29.

Beguería, S., Vicente-Serrano, S. M., Reig, F. & Latorre, B. 2014 Standardized precipitation evapotranspiration index (SPEI) revisited: parameter fitting, evapotranspiration models, tools, datasets and drought monitoring. *International Journal of Climatology* **34** (10), 3001–3023.

Bisht, D. S., Sridhar, V., Mishra, A., Chatterjee, C. & Raghuwanshi, N. S. 2019 Drought characterization over India under projected climate scenario. *International Journal of Climatology* **39** (4), 1889–1911.

Brans, J.-P., Vincke, P. & Mareschal, B. 1986 How to select and how to rank projects: the PROMETHEE method. *European Journal of Operational Research* **24** (2), 228–238.

Burke, E. J. & Brown, S. J. 2010 Regional drought over the UK and changes in the future. *Journal of Hydrology* **394** (3–4), 471–485.

Chen, H. & Sun, J. 2017 Characterizing present and future drought changes over eastern China. *International Journal of Climatology* **37**, 138–156.

Christensen, J. H., Boberg, F., Christensen, O. B. & Lucas-Picher, P. 2008 On the need for bias correction of regional climate change projections of temperature and precipitation. *Geophysical Research Letters* **35** (20), L20709.

Dai, A. 2011 Drought under global warming: a review. *Wiley Interdisciplinary Reviews: Climate Change* **2** (1), 45–65.

Dai, A. 2013 Increasing drought under global warming in observations and models. *Nature Climate Change* **3** (1), 52.

Dai, A., Trenberth, K. E. & Qian, T. 2004 A global dataset of Palmer Drought Severity Index for 1870–2002: relationship with soil moisture and effects of surface warming. *Journal of Hydrometeorology* **5** (6), 1117–1130.

D'Andrea, F., Drobinski, P. & Stéfanon, M. 2016 European heat waves: the effect of soil moisture, vegetation, and land use. *Dynamics and Predictability of Large-Scale, High-Impact Weather and Climate Events 2*, p. 185.

Douville, H. 2002 Influence of soil moisture on the Asian and African monsoons. Part II: interannual variability. *Journal of Climate* **15** (7), 701–720.

Douville, H., Colin, J., Krug, E., Cattiaux, J. & Thao, S. 2016 Midlatitude daily summer temperatures reshaped by soil moisture under climate change. *Geophysical Research Letters* **43** (2), 812–818.

Elía, R. d., Laprise, R., Biner, S. & Merleau, J. 2017 Synchrony between reanalysis-driven RCM simulations and observations: variation with time scale. *Climate Dynamics* **48** (7–8), 2597–2610.

Feng, S., Trnka, M., Hayes, M. & Zhang, Y. 2017 Why do different drought indices show distinct future drought risk outcomes in the US Great Plains? *Journal of Climate* **30** (1), 265–278.

Field, C. B., Barros, V., Stocker, T. F. & Dahe, Q. 2012 *Managing the Risks of Extreme Events and Disasters to Advance Climate Change Adaptation: Special Report of the Intergovernmental Panel on Climate Change*. Cambridge University Press.

Fowler, H., Ekström, M., Blenkinsop, S. & Smith, A. 2007 Estimating change in extreme European precipitation using a multimodel ensemble. *Journal of Geophysical Research: Atmospheres* **112**, D18.

Gerken, T., Bromley, G. T., Ruddell, B. L., Williams, S. & Stoy, P. C. 2018 Convective suppression before and during the United States Northern Great Plains flash drought of 2017. *Hydrology and Earth System Sciences* **22** (8), 4155–4163.

Ghorbani, M. A., Kazempour, R., Chau, K. W., Shamshirband, S. & Taherei Ghazvinei, P. 2018 Forecasting pan evaporation with an integrated Artificial Neural Network Quantum-behaved Particle Swarm Optimization model: a case study in Talesh, Northern Iran. *Engineering Applications of Computational Fluid Mechanics* **12** (1), 724–737.

Greve, P., Orlowsky, B., Mueller, B., Sheffield, J., Reichstein, M. & Seneviratne, S. I. 2014 Global assessment of trends in wetting and drying over land. *Nature Geoscience* **7** (10), 716–721.

Hargreaves, G. H. 1994 Defining and using reference evapotranspiration. *Journal of Irrigation and Drainage Engineering* **120** (6), 1132–1139.

Hernandez, E. A. & Uddameri, V. 2014 Standardized precipitation evaporation index (SPEI)-based drought assessment in semi-arid south Texas. *Environmental Earth Sciences* **71** (6), 2491–2501.

Hersbach, H. 2016 The ERA5 atmospheric reanalysis. *AGU Fall Meeting Abstracts*, NG33D-01.

Hirabayashi, Y., Mahendran, R., Koirala, S., Konoshima, L., Yamazaki, D., Watanabe, S., Kim, H. & Kanae, S. 2013 Global flood risk under climate change. *Nature Climate Change* **3** (9), 816.

Kang, H. & Sridhar, V. 2017 Combined statistical and spatially distributed hydrological model for evaluating future drought indices in Virginia. *Journal of Hydrology: Regional Studies* **12**, 253–272.

Krause, P., Boyle, D. & Bäse, F. 2005 Comparison of different efficiency criteria for hydrological model assessment. *Advances in Geosciences* **5**, 89–97.

Kumar, D. N. 2010 *Multicriterion Analysis in Engineering and Management*. PHI Learning Pvt. Ltd.

Lauer, A., Eyring, V., Righi, M., Buchwitz, M., Defourny, P., Evaldsson, M., Friedlingstein, P., de Jeu, R., de Leeuw, G., Loew, A. & Merchant, C. J. 2017 Benchmarking CMIP5 models with a subset of ESA CCI Phase 2 data using the ESMValTool. *Remote Sensing of Environment* **203**, 9–39.

Liu, Z., Wang, Y., Shao, M., Jia, X. & Li, X. 2016 Spatiotemporal analysis of multiscalar drought characteristics across the Loess Plateau of China. *Journal of Hydrology* **534**, 281–299.

Maity, R., Aggarwal, A. & Chanda, K. 2016a Do CMIP5 models hint at a warmer and wetter India in the 21st century? *Journal of Water and Climate Change* **7** (2), 280–295.

Maity, R., Suman, M. & Verma, N. K. 2016b Drought prediction using a wavelet based approach to model the temporal consequences of different types of droughts. *Journal of Hydrology* **539**, 417–428.

Maity, R., Suman, M., Laux, P. & Kunstmann, H. 2019 Bias correction of zero-inflated RCM precipitation fields: a copula-based scheme for both mean and extreme conditions. *Journal of Hydrometeorology* **20** (4), 595–611.

Mallya, G., Mishra, V., Niyogi, D., Tripathi, S. & Govindaraju, R. S. 2016 Trends and variability of droughts over the Indian monsoon region. *Weather and Climate Extremes* **12**, 43–68.

Maraun, D., Shepherd, T. G., Widmann, M., Zappa, G., Walton, D., Gutiérrez, J. M., Hagemann, S., Richter, I., Soares, P. M., Hall, A. & Mearns, O. L. 2017 Towards process-informed bias correction of climate change simulations. *Nature Climate Change* **7** (11), 764.

Ministry of Finance, India 2018 Economic Survey 2017-18. Tech. Rep. GOI. Available from: http://mofapp.nic.in:8080/economicsurvey/.

Mishra, A. & Singh, V. P. 2009 Analysis of drought severity-area-frequency curves using a general circulation model and scenario uncertainty. *Journal of Geophysical Research: Atmospheres* **114**, D6.

Mishra, V., Shah, R. & Thrasher, B. 2014 Soil moisture droughts under the retrospective and projected climate in India. *Journal of Hydrometeorology* **15** (6), 2267–2292.

Moss, R. H., Edmonds, J. A., Hibbard, K. A., Manning, M. R., Rose, S. K., Van Vuuren, D. P., Carter, T. R., Emori, S., Kainuma, M., Kram, T. & Meehl, G. A. 2010 The next generation of scenarios for climate change research and assessment. *Nature* **463** (7282), 747.

Naresh, K. M., Murthy, C., Sesha Sai, M. & Roy, P. 2012 Spatiotemporal analysis of meteorological drought variability in the Indian region using standardized precipitation index. *Meteorological Applications* **19** (2), 256–264.

Oguntunde, P. G., Abiodun, B. J. & Lischeid, G. 2017 Impacts of climate change on hydro-meteorological drought over the Volta Basin, West Africa. *Global and Planetary Change* **155**, 121–132.

Ojha, R., Kumar, D. N., Sharma, A. & Mehrotra, R. 2013 Assessing severe drought and wet events over India in a future climate using a nested bias-correction approach. *Journal of Hydrologic Engineering* **18** (7), 760–772.

Pai, D., Sridhar, L., Guhathakurta, P. & Hatwar, H. 2011 District-wide drought climatology of the southwest monsoon season over India based on standardized precipitation index (SPI). *Natural Hazards* **59** (3), 1797–1813.

Pai, D., Sridhar, L., Rajeevan, M., Sreejith, O., Satbhai, N. & Mukhopadhyay, B. 2014 Development of a new high spatial resolution (0.25× 0.25) long period (1901–2010) daily gridded rainfall data set over India and its comparison with existing data sets over the region. *Mausam* **65** (1), 1–18.

Pomerol, J.-C. & Barba-Romero, S. 2012 *Multicriterion Decision in Management: Principles and Practice*, Vol. 25. Springer Science & Business Media, New York.

Raju, K. S. & Kumar, D. N. 2014 Ranking of global climate models for India using multicriterion analysis. *Climate Research* **60** (2), 103–117.

Raju, K. S., Sonali, P. & Kumar, D. N. 2017 Ranking of CMIP5-based global climate models for India using compromise programming. *Theoretical and Applied Climatology* **128** (3–4), 563–574.

Schmidli, J., Frei, C. & Vidale, P. L. 2006 Downscaling from GCM precipitation: a benchmark for dynamical and statistical downscaling methods. *International Journal of Climatology* **26** (5), 679–689.

Seneviratne, S. I., Nicholls, N., Easterling, D., Goodess, C. M., Kanae, S., Kossin, J., Luo, Y., Marengo, J., McInnes, K., Rahimi, M. & Reichstein, M. 2012 Changes in climate extremes and their impacts on the natural physical environment. In: *Managing the Risks of Extreme Events and Disasters to Advance Climate Change Adaptation: Special Report of the Intergovernmental Panel on Climate Change*. Cambridge University Press, New York,, pp. 109–230.

Shamshirband, S., Hashemi, S., Salimi, H., Samadianfard, S., Asadi, E., Shadkani, S., Kargar, K., Mosavi, A., Nabipour, N. & Chau, K. W. 2020 Predicting standardized streamflow index for hydrological drought using machine learning models. *Engineering Applications of Computational Fluid Mechanics* **14** (1), 339–350.

Sharma, S. & Mujumdar, P. 2017 Increasing frequency and spatial extent of concurrent meteorological droughts and heatwaves in India. *Scientific Reports* **7** (1), 15582.

Sharma, T., Vittal, H., Chhabra, S., Salvi, K., Ghosh, S. & Karmakar, S. 2018 Understanding the cascade of GCM and

downscaling uncertainties in hydro-climatic projections over India. *International Journal of Climatology* **38**, e178–e190.

Sheffield, J. & Wood, E. F. 2008 Projected changes in drought occurrence under future global warming from multi-model, multi-scenario, IPCC AR4 simulations. *Climate Dynamics* **31** (1), 79–105.

Sheffield, J., Wood, E. F. & Roderick, M. L. 2012 Little change in global drought over the past 60 years. *Nature* **491** (7424), 435–438.

Spinoni, J., Vogt, J. V., Naumann, G., Barbosa, P. & Dosio, A. 2018 Will drought events become more frequent and severe in Europe? *International Journal of Climatology* **38** (4), 1718–1736.

Stevens, B. & Bony, S. 2013 What are climate models missing? *Science* **340** (6136), 1053–1054.

Stocker, T. F., Qin, D., Plattner, G., Tignor, M., Allen, S., Boschung, J., Nauels, A., Xia, Y., Bex, V. & Midgley, P. 2013 Climate change 2013: the physical science basis. In Working Group I Contribution to the Fifth Assessment Report of the Intergovernmental Panel on Climate Change 2013. Tech. Rep. Intergovernmental Panel on Climate Change.

Suman, M. & Maity, R. 2016 Foreseeing the agricultural and hydrological drought knowing the ongoing meteorological scenarios through wavelet analysis. In: *Proceedings of the International Conference on Hydraulics, Water Resources, Coastal & Environmental Engineering*. The Indian Society for Hydraulics, Pune, India.

Suman, M. & Maity, R. 2020 Southward shift of precipitation extremes over south Asia: evidences from CORDEX data. *Scientific Reports* **10** (1), 1–11. doi:10.1038/s41598-020-63571-x.

Taylor, K. E. 2001 Summarizing multiple aspects of model performance in a single diagram. *Journal of Geophysical Research: Atmospheres* **106** (D7), 7183–7192.

Teutschbein, C. & Seibert, J. 2010 Regional climate models for hydrological impact studies at the catchment scale: a review of recent modeling strategies. *Geography Compass* **4** (7), 834–860.

Thomas, T., Nayak, P. & Ghosh, N. C. 2015 Spatiotemporal analysis of drought characteristics in the Bundelkhand region of central India using the standardized precipitation index. *Journal of Hydrologic Engineering* **20** (11), 05015004.

Thrasher, B., Maurer, E. P., Duffy, P. B. & McKellar, C. 2012 *Bias Correcting Climate Model Simulated Daily Temperature Extremes with Quantile Mapping*. Tech. Rep. Copernicus Publications on behalf of the European Geosciences Union.

Trenberth, K. E. 2011 Changes in precipitation with climate change. *Climate Research* **47** (1/2), 123–138.

Trenberth, K. E., Dai, A., Rasmussen, R. M. & Parsons, D. B. 2003 The changing character of precipitation. *Bulletin of the American Meteorological Society* **84** (9), 1205–1217.

Vicente-Serrano, S. M., Beguería, S. & López-Moreno, J. I. 2010 A multiscalar drought index sensitive to global warming: the standardized precipitation evapotranspiration index. *Journal of Climate* **23** (7), 1696–1718.

Vicente-Serrano, S. M., Lopez-Moreno, J.-I., Beguería, S., Lorenzo-Lacruz, J., Sanchez-Lorenzo, A., García-Ruiz, J. M., Azorin-Molina, C., Morán-Tejeda, E., Revuelto, J., Trigo, R. & Coelho, F. 2014 Evidence of increasing drought severity caused by temperature rise in southern Europe. *Environmental Research Letters* **9** (4), 044001.

Wang, H., Chen, Y., Pan, Y. & Li, W. 2015 Spatial and temporal variability of drought in the arid region of China and its relationships to teleconnection indices. *Journal of Hydrology* **523**, 283–296.

Willmott, C. J., Robeson, S. M. & Matsuura, K. 2012 A refined index of model performance. *International Journal of Climatology* **32** (13), 2088–2094.

Xu, K., Yang, D., Yang, H., Li, Z., Qin, Y. & Shen, Y. 2015 Spatio-temporal variation of drought in China during 1961–2012: a climatic perspective. *Journal of Hydrology* **526**, 253–264.

Yuan, X., Wang, L., Wu, P., Ji, P., Sheffield, J. & Zhang, M. 2019 Anthropogenic shift towards higher risk of flash drought over China. *Nature Communications* **10** (1), 1–8.

Zhang, X., Obringer, R., Wei, C., Chen, N. & Niyogi, D. 2017 Droughts in India from 1981 to 2013 and implications to wheat production. *Scientific Reports* **7**, 44552.

Zhao, C., Huang, Y., Li, Z. & Chen, M. 2018 Drought monitoring of southwestern China using insufficient GRACE data for the long-term mean reference frame under global change. *Journal of Climate* **31** (17), 6897–6911.

First received 31 December 2020; accepted in revised form 26 February 2021. Available online 18 March 2021